

Losses in Multilevel Crossover in VLSI Interconnects

P.K.Datta*, S.Sanyal[†] and D.Bhattacharya[‡]

Department of Electronics & Electrical Communication Engineering
Indian Institute of Technology, Kharagpur, India

e-mail: *prabir@ece.iitkgp.ernet.in, [†]ssanyal@ece.iitkgp.ernet.in and [‡]dilip@ece.iitkgp.ernet.in

Abstract

The radiation and surface wave losses may give rise to electromagnetic interference (EMI) problems in high speed VLSI interconnects. Over and above there will be dielectric and conductor losses. These losses have been evaluated for multilevel interconnects by finite difference time domain (FDTD) technique. The crosstalk between lines in the same level as well as in different levels and propagation delays are also found.

1. Introduction

Today's high speed VLSI interconnects are having multilevel structures and designers feel concerned about losses induced by planar lines and discontinuities. Over and above the conductor and dielectric losses, the planar lines with discontinuities exhibit losses due to surface waves and space waves. These losses degrade the signal distribution and may lead to electromagnetic interference (EMI) problem and similar other unwanted effects. Several literatures are available where losses in microstrip lines including radiation and surface wave losses from discontinuities are found [1]-[7]. But no such information for multilevel structures is available. This paper aims at evaluating the conductor loss, dielectric loss, radiation loss and surface wave loss in a multiconductor multilevel structure. Multilevel crossover structure has been analyzed in [8] and equivalent circuit has been found. But the model does not account for radiation and surface waves. To account for all these full-wave effects, finite difference time domain (FDTD) technique [9] has been used in this paper. All the frequency dependent full-wave behaviors like dispersion, cross talk, radiation and surface waves are automatically accounted for in FDTD method. Surface impedance boundary condition (SIBC) [10] is used for incorporation of conductor loss. Dielectric loss is taken into account by taking the nonzero conductivity of the substrate. Near field to far field transformation (NFFF) [11] is used for the computation of radiated fields. FDTD method

produces the TDR directly and no tedious parameter extraction or Fourier transform is required. From the voltages at different ports the propagation delays are calculated.

Crossover structures with and without bend, (shown in fig. 1) are analyzed in this paper. For truncation of the FDTD computation domain uniaxial perfectly matched layer (UPML) boundary [12] is used. Non-uniform grid FDTD scheme [13] is used as it saves memory and computer time.

2. Formulation

2.1. Uniaxial perfectly matched layer (UPML) boundary

Within the FDTD computation domain the fields are updated using Yee algorithm [9]. The computation domain is truncated by UPML boundary. In the UPML regions the fields are updated in two steps and non-split field formulation is used. Within the UPML regions the two-step update equations for E^z field component are obtained following the method illustrated in [12] as

$$D_{z_{i,j,k+\frac{1}{2}}}^{n+\frac{1}{2}} = \left(\frac{A_1}{A_2}\right) D_{z_{i,j,k+\frac{1}{2}}}^{n-\frac{1}{2}} + \left(\frac{1}{A_2}\right) (A_3 - A_4) \quad (1)$$

$$E_{z_{i,j,k+\frac{1}{2}}}^{n+\frac{1}{2}} = \left(\frac{C_1}{C_2}\right) E_{z_{i,j,k+\frac{1}{2}}}^{n-\frac{1}{2}} + \left(\frac{1}{C_2\epsilon_0\epsilon_r}\right) (C_3 - C_4) \quad (2)$$

where,

$$\begin{aligned} A_1 &= \frac{\kappa_x}{\Delta t} - \frac{\sigma_x}{2\epsilon_0\epsilon_r} \\ A_2 &= \frac{\kappa_x}{\Delta t} + \frac{\sigma_x}{2\epsilon_0\epsilon_r} \\ A_3 &= \frac{H_{y_{i+\frac{1}{2},j,k+\frac{1}{2}}}^n - H_{y_{i-\frac{1}{2},j,k+\frac{1}{2}}}^n}{\Delta x} \\ A_4 &= \frac{H_{x_{i,j+\frac{1}{2},k+\frac{1}{2}}}^n - H_{x_{i,j-\frac{1}{2},k+\frac{1}{2}}}^n}{\Delta y} \end{aligned}$$

$$\begin{aligned}
C_1 &= \kappa_y - \frac{\sigma_y}{2\epsilon_0\epsilon_r} \\
C_2 &= \kappa_y + \frac{\sigma_y}{2\epsilon_0\epsilon_r} \\
C_3 &= \left(\kappa_z + \frac{\sigma_z\Delta t}{2\epsilon_0\epsilon_r} \right) D^{z_{i,j,k+\frac{1}{2}}^{n+\frac{1}{2}}} \\
C_4 &= \left(\kappa_z - \frac{\sigma_z\Delta t}{2\epsilon_0\epsilon_r} \right) D^{z_{i,j,k+\frac{1}{2}}^{n-\frac{1}{2}}}
\end{aligned}$$

When $\kappa_x = \kappa_y = \kappa_z = 1$ then (1) and (2) take the form given in [12]. Gedney has suggested the use of $\kappa_i > 1$; (i = x, y or z) for better absorption of evanescent waves. To take advantage of this fact the expressions given by Gedney have been modified by incorporating κ_i . Similar two-step update equations can be found for other field components. The conductivity σ , permittivity ϵ and permeability μ are scaled within the UPML region in the normal direction while in the transverse directions they are kept same as the corresponding values in the computation domain. In the x direction, when this is normal to the UPML interface, σ_x and $\epsilon_x = \mu_x = \kappa_x$ are varied following the equations

$$\sigma_x(x) = \sigma_{x_{max}} \left(\frac{x}{d} \right)^m \quad (3)$$

$$\kappa_x(x) = 1 + \kappa_{x_{max}} \left(\frac{x}{d} \right)^m \quad (4)$$

where, d is the depth of the UPML region and m is the polynomial scaling factor. $\sigma_{x_{max}}$ and $\kappa_{x_{max}}$ are the maximum values of σ_x and $\epsilon_x = \mu_x = \kappa_x$ respectively at the outer face of the UPML boundary. The optimum value of $\sigma_{x_{max}}$ is given in [12] as

$$\sigma_{x_{max}} = \frac{m+1}{150\pi\sqrt{\epsilon_{eff}}} \quad (5)$$

where, ϵ_{eff} is the effective dielectric constant of the microstrip. The equations for other normal directions are similar to (1)-(5). In the rest of the paper the subscripts indicating normal directions are omitted and it is assumed that they are in any of the three directions, whichever is appropriate. The optimum values of κ_{max} are found following [14].

2.2. Surface impedance boundary condition (SIBC)

For incorporation of conductor loss in FDTD, SIBC is used. For implementation of SIBC the method given in [10] is adopted in this paper. Due to the frequency dependent nature of surface impedance, convolution is required in time domain. The surface impedance in the Laplace domain is

$$Z_c(s) = \eta \sqrt{\frac{s/a}{1+s/a}} \quad (6)$$

where, $a = \sigma/\epsilon$ and $\eta = \sqrt{\mu/\epsilon}$; σ is the conductivity of strip and ground plane conductors and the substrate have permittivity ϵ and permeability μ . Defining $s' = s/a$ the normalized surface impedance is

$$Z_n(s') = Z_c(as')/\eta = \sqrt{s'/(1+s')} \quad (7)$$

The normalized surface impedance $Z_n(s')$ is approximated by first order rational functions as

$$Z_n(s') = 1 - \sum_{i=1}^N c_i/(s' + \omega_i) \quad (8)$$

where, N is the number of first order rational function used in the approximation. The values of c_i and ω_i are found by least square method. It is shown in [10] that with N = 8 the maximum relative error in $Z_n(s')$ is 0.0016 %. As s' is independent of material and geometrical parameters, the values of c_i and ω_i have to be computed once only and those values can be used for all simulations. In time domain the tangential electric and magnetic fields at the conductor-dielectric interface are related by

$$E_t(t) = Z_c(t) * [\hat{n} \times H_t(t)] \quad (9)$$

where, * denotes convolution. $Z_c(t)$ can be found by inverse Laplace transform of (8). Assuming the waves to be piecewise linear in time and implementing recursive convolution, the update equation for tangential electric fields are

$$E_t(n\Delta t) = \eta[\hat{n} \times H_t(n\Delta t)] - \sum_{i=1}^N F_i(n\Delta t) \quad (10)$$

where,

$$\begin{aligned}
F_i(n\Delta t) &= p_{i1}[\hat{n} \times H_t(n\Delta t)] + p_{i2}[\hat{n} \times H_t\{(n-1)\Delta t\}] \\
&\quad + p_{i3}F_i\{(n-1)\Delta t\}
\end{aligned}$$

$$p_{i1} = \frac{\eta c_i}{\omega_i} \left[1 + \frac{(e^{-q} - 1)}{q} \right]$$

$$p_{i2} = \frac{\eta c_i}{\omega_i} \left[\frac{1}{q} - e^{-q} \left(1 + \frac{1}{q} \right) \right]$$

$$p_{i3} = e^{-q}$$

$$q = a\omega_i\Delta t$$

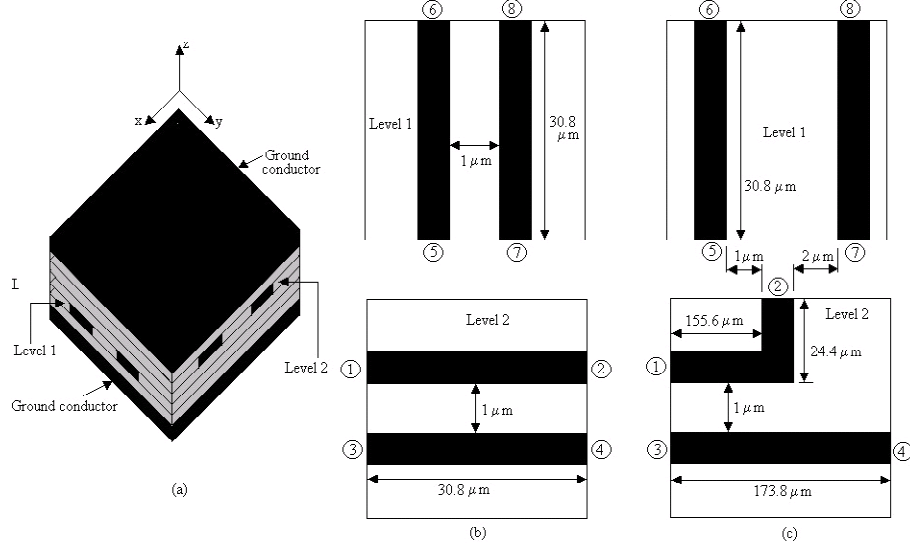


Figure 1. Multilevel crossover. (a) 3-D view. SiO_2 and conductors are shown in gray and black respectively. Five SiO_2 layers ($\epsilon_r=3.9$) are $1 \mu m$ thick and the copper conductor ($\sigma = 4.1 \times 10^7 Sm^{-1}$) strips are of width $1 \mu m$ and thickness $1 \mu m$. **(b) Crossover without bend. (c) Crossover with bend.** In (b) and (c) numbers within circle indicate port number.

2.3. Near field to far field transform (NFFF) and the radiated fields

The far field will contain only $\hat{\theta}$ and $\hat{\phi}$ components. For evaluation of radiated far field, a surface called near field to far field surface is taken which is inside the computation domain and encompasses the structure. The six faces of the near field to far field surface are divided into patches by the FDTD grid. The tangential electric and magnetic fields at the center of each patch are found by taking average of adjacent fields. The scheme for computation of far field is detailed in [11]. The time domain far fields are Fourier transformed to obtain frequency domain far fields $E_{\theta}(\omega)$ and $E_{\phi}(\omega)$. Integrating these fields the radiated power is found as

$$R(\omega) = \frac{\pi r^2}{\eta} \int_0^{2\pi} \int_0^{\pi} [|E_{\theta}(\omega)|^2 + |E_{\phi}(\omega)|^2] \sin(\theta) d\theta d\phi \quad (11)$$

where, $\eta=120\pi$ is the free space wave impedance.

3. Numerical results

Crossovers, with and without bend, are analyzed in this paper. The structures are shown in fig. 1. The two-level crossover has two conductors in each level. The conductors are of Copper (conductivity $\sigma = 4.1 \times 10^7 Sm^{-1}$) with width $1 \mu m$ and thickness $1 \mu m$. The five SiO_2 layers are

of thickness $1 \mu m$ and $\epsilon_r=3.9$ and covered by two ground conductors (copper) of thickness $1 \mu m$ on both top and bottom. This structure is taken from [15]. The line lengths and separations are shown in fig. 1. The excitation pulse is trapezoidal with rise-time and fall-time $\tau_r = \tau_f=380$ fs and on-time $\tau_{on}=380$ fs. The TDR are shown in figs. 2 and 3 for crossovers without bend and with bend respectively. A major portion of the incident power is transmitted through the excited line and reaches port 2. The propagation delays for the signal to reach from port 1 to port 2 are 1.2 ps and 0.2 ps respectively for with and without bend case. There is considerable coupling between the lines in the same level as well as between lines in different levels. These coupled signal amplitudes are nearly 10 % of that of the incident pulse. Due to presence of bend, reflection is observed in V_1 for the crossover with bend structure. This reflection is not present in the crossover without bend structure. Due to the bend, a significant crosstalk is observed in V_3 after around 2 ps.

The conductor and dielectric losses are shown in fig. 4. For computation of conductor and dielectric losses the structure taken has only one line in level 2 and no line in level 1. For computation of dielectric loss the conductivity of SiO_2 is taken to be $\sigma_d = 1.0 \times 10^{-4} Sm^{-1}$ while the conductivity of conducting lines are set to a very high value ($\sigma_c = 1.0 \times 10^{70} Sm^{-1}$). For evaluation of conductor loss, $\sigma_d = 0$ and $\sigma_c = 4.1 \times 10^7 Sm^{-1}$. It can be seen that at all frequencies the conductor loss is higher compared to dielectric loss. This higher conductor loss is as expected [1].

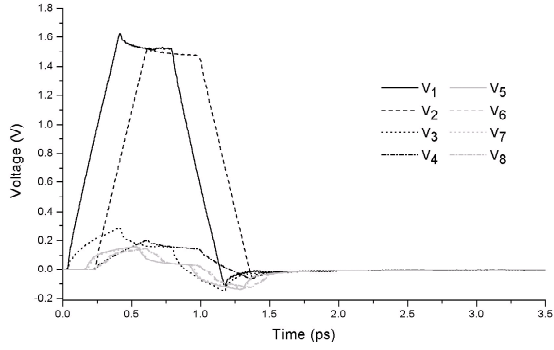


Figure 2. Voltages at different ports of the crossover without bend. Excitation is given at port 1 with a trapezoidal pulse of $\tau_r = \tau_f = \tau_{on} = 380$ fs. V_i indicates voltage at port i . Upper graph (V_1 to V_4) shows voltages in level 2 and the lower graph (V_5 to V_8) shows voltages in level 1.

For comparison purpose, the conductor loss for microstrip on alumina ($\epsilon_r=9.9$ and height $h=0.64$ mm) with strip width $w = 0.04$ mm is plotted in the inset of fig. 4 along with the result given in [1]. This shows good match between our result and the result of [1].

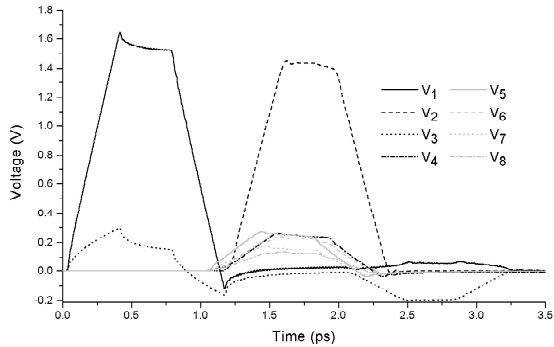


Figure 3. Voltages at different ports of the crossover with bend. Excitation is given at port 1 with a trapezoidal pulse of $\tau_r = \tau_f = \tau_{on} = 380$ fs. V_i indicates voltage at port i . Upper graph (V_1 to V_4) shows voltages in level 2 and the lower graph (V_5 to V_8) shows voltages in level 1.

For the computation of radiation loss, the crossover with bend structure is taken. The top conducting ground plane is removed so that the structure can radiate. The simulation has been performed for zero conductor and dielectric losses. The structure is excited by Gaussian pulse with

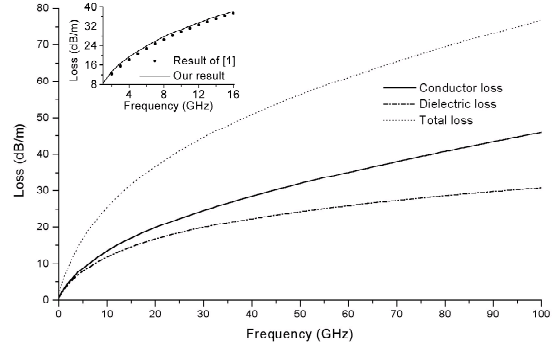


Figure 4. Conductor and dielectric losses for a straight conductor placed on level 2 and no conductor in level 1. The structure has five SiO_2 layers ($\epsilon_r=3.9$, $\sigma_d = 1.0 \times 10^{-4} Sm^{-1}$) of thickness $1 \mu m$. The conducting strip is of copper ($\sigma_c = 4.1 \times 10^7 Sm^{-1}$) of width $1 \mu m$ and thickness $1 \mu m$. Inset: Comparison of conductor loss for a single microstrip line on alumina ($\epsilon_r=9.9$ and height $h=0.64$ mm) with strip width $w=0.04$ mm with the result of [1].

$\tau_r=380$ fs. The radiated power as a function of frequency is plotted in fig. 5. The S-parameters are also computed for the crossover with bend that have zero conductor and dielectric losses. From $1 - \sum |S_{ij}|^2$; $i = 1, 2, \dots, 8$ and $j = 1$; the total loss is found. As there is no conductor and dielectric losses, this total loss is due to radiation and surface wave losses. Thus FDTD computed normalized radiated power when subtracted from the total loss gives surface wave loss. The total loss and surface wave loss are also shown in fig. 5. At low frequencies the surface wave loss is higher and both radiation and surface wave losses increases with frequencies. But beyond 91 GHz radiation loss becomes higher compared to surface wave loss.

4. Conclusion

Different losses are found in this paper for multilevel crossover with and without bend. Conductor loss is higher compared to dielectric loss for these structures. For crossover with bend there is considerable radiation loss and this loss increases with frequency. There is also problem of surface waves. These radiation and surface waves may give rise to EMI problems. Pulse responses of multilevel crossovers have been computed directly and thus no Fourier transform or tedious parameter extraction is required.

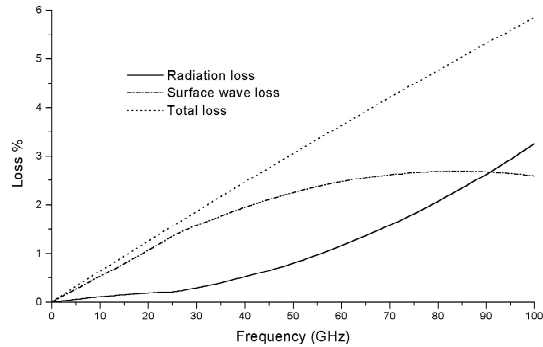


Figure 5. Total loss, radiation loss and surface wave loss for the crossover with bend. Conductor and dielectric losses are assumed zero.

References

- [1] R. H. Jansen, "High-speed computation of single and coupled microstrip parameters including dispersion, high-order modes, loss and finite strip thickness," *IEEE Trans. Microwave Theory and Tech.*, Vol. 26, pp. 75-82, Feb. 1978.
- [2] E.J. Denlinger, "Losses in microstrip lines," *IEEE Trans. Microwave Theory and Tech.*, Vol. 28, pp. 513-522, June 1980.
- [3] L. Lewin, "Radiation from discontinuities in strip-line," *Proc. IEE, Part H*, pp. 163-170, Feb. 1960.
- [4] T. Horng, S. Wu, H. Yang and N.G. Alexopoulos, "A generalized method for distinguishing between radiation and surface-wave losses in microstrip discontinuities," *IEEE Trans. Microwave Theory and Tech.*, Vol. 38, pp. 1800-1807, Dec. 1990.
- [5] W.P. Harokopus, L.P.B. Katehi, W.Y. Ali-Ahmad and G.M. Rebeiz, "Surface wave excitation from open end microstrip discontinuities," *IEEE Trans. Microwave Theory and Tech.*, Vol. 39, pp. 1098-1107, July 1991.
- [6] N. Feix, M. Lalande and B. Jecko, "Harmonical characterization of a microstrip bend via the finite difference time domain method," *IEEE Trans. Microwave Theory and Tech.*, Vol. 40, pp. 955-961, May 1992.
- [7] E. Takagi, B. Houshmand and T. Itoh, "Practical metal loss implementation for a microstrip line structure using SIBC in FDTD simulation," *MTT-S International Microwave Symposium Digest 1997*, Vol. III, pp. 1531-1534.
- [8] A. K. Goel, *High-speed VLSI interconnections*, John Wiley and Sons Inc., New York, 1994.
- [9] K.S.Yee, "Numerical solution of initial boundary value problems involving Maxwell's equation in isotropic media," *IEEE Trans. Antennas and Propagation*, Vol. 14, pp. 302-307, May 1966.
- [10] K. Suk and J. E. Schutt-Aine, "An efficient implementation of surface impedance boundary condition for the finite-difference time-domain method," *IEEE Trans. Antennas Propagation*, Vol. 43, pp. 660-666, July 1995.
- [11] A. Taflov, *Advances in computational electrodynamics*, Artech House, Norwood, MA, 1998, chapter 7.
- [12] S. D. Gedney, "An anisotropic perfectly matched layer-absorbing medium for the truncation of FDTD lattices," *IEEE Trans. Antennas and Propagation*, Vol. 44, pp. 1630-1639, Dec. 1996.
- [13] S. D. Gedney and F. Lansing, "Explicit time-domain solution of Maxwell's equations using nonorthogonal and unstructured grids," *Computational electrodynamics the finite-difference time-domain method*, A. Taflov, Artech House, Norwood, MA, 1995, Chap. 11.
- [14] Z. Ma, and Y. Kobayashi, "Performance of modified PML absorbing boundary condition for propagating and evanescent waves in three-dimensional structures," *IEICE Trans Electron*, Vol. E81C, pp. 1892-1897, Dec. 1998.
- [15] W. Hong, W. Sun, Z. Zhu, H. Ji, B. Song, and W. W. Dai, "A novel dimension-reduction technique for the capacitance extraction of 3-D VLSI interconnects" *IEEE Trans. Microwave Theory and Tech.*, Vol. 46, pp. 1037-1044, Aug. 1998.